ELSEVIER

Journal of Nuclear Materials 289 (2001) 227–242

journal of nuclear materials

www.elsevier.nl/locate/jnucmat

Investigation of models to predict the corrosion of steels in flowing liquid lead alloys

F. Balbaud-Célérier *, F. Barbier

Service de la Corrosion, d'Electrochimie et de Chimie des Fluides, CEA-Saclay, 91191, Gif sur Yvette cedex, France

Received 16 November 2000; accepted 5 January 2001

Abstract

Corrosion of steels exposed to flowing liquid lead alloys can be affected by hydrodynamic parameters. The rotating cylinder system is of interest for the practical evaluation of the fluid velocity effect on corrosion and for the prediction of the corrosion behavior in other geometries. Models developed in aqueous medium are tested in the case of liquid metal environments. It is shown that equations established for the rotating cylinder and the pipe flow geometry can be used effectively in liquid lead alloys (Pb–17Li) assuming the corrosion process is mass transfer controlled and the diffusion coefficient of dissolved species is known. The corrosion rate of martensitic steels in Pb–17Li is shown to be independent of the geometry when plotted as a function of the mass transfer coefficient. Predictions about the corrosion of steel in liquid Pb–Bi are performed but experiments are needed to validate the results obtained by modeling.

1. Introduction

Accelerator driven systems are a technical option to transmute plutonium, minor actinides and long-lived fission products into short-lived radioisotopes or stable nuclei. In such systems, protons generated from an accelerator impinge on a target to produce neutrons by a spallation process. These neutrons are then used for waste transmutation. Flowing liquid metals are primary candidates for the spallation target material due to the high power density deposited by the proton beam. The lead–bismuth eutectic (Pb–55 at.% Bi) appears to be a good candidate due to its high atomic number, low melting point, fast heat removal from the target, good neutron yield and low vapor pressure. It is chemically inert and does not react with air or water violently.

One of the concerns with the use of liquid metals is their compatibility with the containment structure. Liquid metal corrosion can proceed via various processes: dissolution, formation of intermetallic compounds at the interface, penetration of liquid metal along grain boundaries, which depend on experimental factors such as: temperature, thermal gradients, solid and liquid compositions, velocity of the liquid metal.

From studies carried out in flowing lead–lithium alloy (candidate material for the liquid breeding blanket of fusion reactors), it is known that the corrosion rate of martensitic steels, at 475°C (hot leg temperature) and for a temperature gradient of 60°C (cold leg temperature = 415°C), increases from 21 to 93 μm yr^{-1} when the alloy velocity increases from 0.019 to 0.18 m s^{-1} [1]. In the spallation module, the velocity of liquid lead–bismuth could reach values up to 3 m s^{-1} (in our study we will consider a larger velocity range with values up to 5 m s^{-1}) [2]. Therefore, it appears necessary to consider the hydrodynamic effects and to study thoroughly the influence of the liquid Pb–Bi velocity on the corrosion of structural materials for selection of the container.

For practical evaluation of the Pb–Bi velocity effect on the corrosion of steels, an experimental device is being built at the laboratory, which consists in a rotating cylinder operating under controlled hydrodynamic conditions [3]. The major question is how the results obtained on the rotating cylinder can be used to predict

* Corresponding author. Tel.: + 33-1 69 08 16 51; fax: + 33-1 69 08 15 86.

E-mail address: fanny.balbaud@cea.fr (F. Balbaud-Célérier).

0022-3115/01/$ - see front matter
PII: S0022-3115(01)00431-7

the behavior of the materials in the hydrodynamic and geometric conditions of the spallation module.

Several models have been developed in aqueous media (especially in the field of the oil and gas industries) to predict the fluid velocity effects on corrosion from the results obtained with a rotating cylinder [4–14]. However, very few studies have been performed in liquid metals and the purpose of this paper is to determine if the existing models can be used in the case of liquid metals or if new equations are necessary for this specific application.

Within the context of the fusion reactors studies, corrosion of steels in the presence of flowing lead–lithium alloy (Pb–17 at.% Li) has been widely studied by means of pipe loops and rotating cylinder specimens. Therefore, it is possible to determine if the models proposed in the literature for aqueous media can be considered in the case of liquid metals by using the experimental results obtained in Pb–17Li via loops and rotating cylinder specimens. An analysis will also be carried out in pure liquid lead by using some corrosion data. Then, the best appropriate equations will be used to perform a first evaluation of the corrosion behavior of steels in contact with flowing Pb–Bi in the spallation module.

It has to be noted that the corrosion rate of steels exposed to Pb or Pb–Bi depends on the concentration of oxygen dissolved in the liquid alloy [15]. At high oxygen content, an oxide layer can be formed on the steel surface (lead oxides are less stable than iron oxides), which protects it from corrosion. At low oxygen content, there is no oxidation and corrosion occurs by dissolution of the steel components in the liquid metal. In this paper, only the latter case will be discussed. However, hydrodynamic factors can also affect the external surface of the oxide layer in contact with the flowing liquid metal depending on the characteristics of this layer: porosity, solubility. For example, a high fluid velocity could generate the erosion of a porous oxide layer leaving the metal unprotected.

2. Modeling of flow-induced corrosion

2.1. Generalities

This section briefly introduces the hydrodynamic factors that affect the corrosion rate.

When a liquid interacts with a solid wall, there are different regions to consider for velocity distribution in a turbulent flow (in the spallation module, due to the high fluid velocities, the flow is turbulent) [6,16]:

– A thin laminar sublayer of thickness δ_h resulting from viscous drag is present close to the pipe surface. In this region, the flow is stabilized by the presence of the wall and remains laminar.
– A fully turbulent region, in which the highest velocities are obtained.
– A buffer layer between the laminar sublayer and the fully turbulent region. This region is characterized by turbulent conditions which are of lower intensity than in the fully turbulent region.

Moreover, if mass transport occurs at the surface, there is also a diffusion boundary layer of thickness δ_d across which there is a concentration gradient [16].

Conventionally, the characteristics of hydrodynamic systems are described by dimensionless numbers such as the Reynolds number (*Re*), the Schmidt number (*Sc*) and the Sherwood number (*Sh*).

The Reynolds number expresses the ratio of the inertial forces acting on a fluid to the viscous forces:

$$Re = \frac{vd}{v},$$

where v is the fluid relevant velocity (m s^{-1}), d is the characteristic specimen length (m) and v is the kinematic viscosity of the fluid (m^2 s^{-1}).

For velocities lower than a critical value characterized by a Reynolds number, $Re_{critical}$, the flow remains laminar. For higher velocities, it becomes turbulent. Table 1 gives the expression of the Reynolds number for various geometries and the transition critical values between laminar and turbulent flow [6].

The relationship between the thickness of the laminar sublayer (δ_h) and the thickness of the diffusion boundary layer (δ_d) is governed by the Schmidt number:

$$Sc = \frac{v}{D},$$

where D is the diffusion coefficient of the relevant species (m^2 s^{-1}).

The higher the value of *Sc*, the thinner will be the diffusion layer and the faster will be its formation.

The Sherwood number is related to the mass transfer which is introduced hereafter.

2.2. Mass transfer

Mass transfer is the process of transporting material from a surface to the bulk of a flowing fluid. The overall transport to the surface consists of diffusion at the interface solid–liquid and bulk convection. This kind of transport is known as convective diffusion. The mass transfer rate can be expressed according to

$$\text{Rate of reaction} = K\Delta c,$$

where K (m s^{-1}) is an empirical mass transfer coefficient depending on hydrodynamic factors and Δc is the concentration gradient between the solid–liquid interface and the bulk [6,17].

In some cases, the mass transfer coefficient is considered to be the ratio D/δ_d where D is the diffusion

Table 1
Reynolds numbers for different specimen geometries [6]

Geometry	Characteristic length (m)	Reynolds number	Critical Reynolds number
Smooth pipe	Inner pipe diameter: d_{pipe}	$\frac{v_{pipe}d_{pipe}}{v}$ v_{pipe} : linear velocity (m s^{-1})	≈ 2000
Rotating disc	Disc radius: r_d	$\frac{\omega r_d^2}{v}$ ω : angular velocity (rad s^{-1})	$\approx 10^5$
Rotating cylinder	External cylinder diameter: $d_{cylinder}$	$\frac{v_{cylinder}d_{cylinder}}{v} = \frac{\omega d_{cylinder}^2}{2v}$ $v_{cylinder}$: peripheral velocity $= \frac{\omega d_{cylinder}}{2}$ (m s^{-1})	≈ 200

coefficient (m^2 s^{-1}) and δ_d (m) is the thickness of the diffusion boundary layer. The thickness of the diffusion layer is a function of the fluid velocity, the geometry of the installation and the physicochemical properties of the fluid.

Mass transfer rates can also be expressed in a dimensionless form by the Sherwood number

$$Sh = \frac{Kd}{D},$$

where K is the mass transfer coefficient (m s^{-1}), d is the characteristic specimen length (m) and D is the diffusion coefficient of the relevant species (m^2 s^{-1}).

It can be shown by dimensional analysis that Sh is a function of Re and Sc. Such relationships can be derived theoretically, however they are usually obtained as empirical correlations of experimental data obtained within certain limits and are usually of the form

$$Sh = aRe^bSc^c,$$

where a, b, and c are empirical constants: b is usually between 0.3 and 1, c is typically 0.33.

2.3. Momentum transfer

Momentum transfer is the physical force within the fluid acting through turbulence at the solid metal surface. It is measured by τ (N m^{-2}), the wall shear stress [14]. This parameter is a direct measurement of the viscous energy loss within the turbulent boundary layer and it is related to the intensity of turbulence in the fluid acting on the wall. Wall shear stress can be expressed as

$$\tau = \frac{f}{2}v^2\rho,$$

where f is the dimensionless Fanning friction factor, v is the fluid velocity (m s^{-1}) and ρ is the fluid density (kg m^{-3}).

To determine the expression of the friction factor, one of the simplest correlation is the Blasius equation [8]:

$$f = 0.079Re^{-0.25} \text{ for } 2.3 \times 10^3 < Re < 10^5.$$

For higher Reynolds numbers and smooth pipes, the expression is [12]

$$\frac{1}{\sqrt{f}} = 4\log\left(Re\sqrt{f}\right) - 0.4 \text{ for } Re > 3000.$$

Another expression gives [8]

$$f = 0.046Re^{-0.2} \text{ for } Re > 10^5.$$

In most cases, the Reynolds number does not exceed 10^5, therefore the Blasius equation is considered.

For the rotating cylinder, the wall shear stress is

$$\tau = \frac{f}{2}\omega^2r^2\rho,$$

where f is the friction factor, ω is the angular velocity (rad s^{-1}) and r is the cylinder external radius (m).

The expression of the friction factor is [8,12]

$$\frac{f}{2} = 0.079Re^{-0.3} \text{ for } Re > 300.$$

The majority of the changes in fluid stress characteristics, turbulence, mass transfer and fluid interaction with the wall occurs in the boundary layer. This implies that a test method allowing calculation of values for geometry-independent parameters acting on the test specimen can be used to investigate fluid flow effects on corrosion for any system that can be characterized hydrodynamically [14].

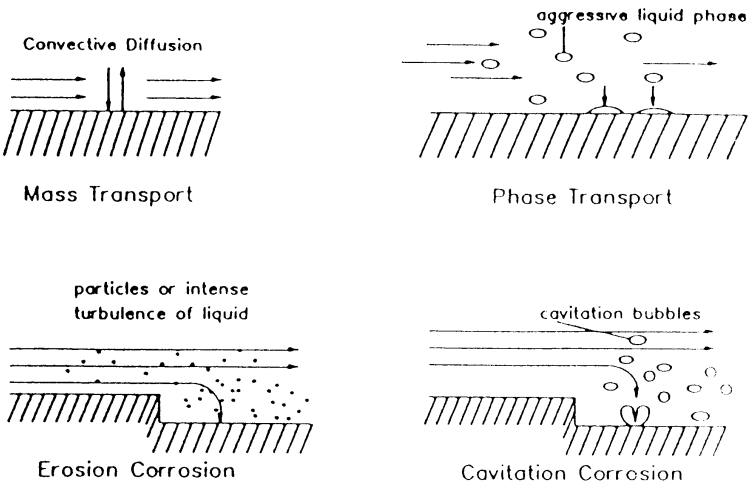

Fig. 1. Representation of the four main types of flow-induced corrosion [17].

2.4. Velocity distribution in a turbulent flow: effect on the corrosion process

The different mechanisms of combined action of flow and corrosion lead to four types of flow-induced corrosion: mass transport-controlled corrosion, phase transport-controlled corrosion, erosion–corrosion and cavitation–corrosion. They are represented on Fig. 1 and the main interactions between a flowing liquid and a solid surface are synthesized on Fig. 2 [17].

The effects of flow velocity may be summarized as follows [18]:

– At flow velocities close to zero, i.e., in the absence of induced convection, natural convection alone is involved in mass transfer.

– Under the influence of moderate induced convection, mass transfer increases but mechanical flow effects are absent.

– When the system is subjected to forced convection with high flow velocities leading to mechanical flow effects, protective films (passive films, layers of corrosion products) and, in extreme cases, the metallic substrate itself may suffer from mechanically induced damage.

In liquid metal environment where corrosion occurs by direct dissolution (which is the case for the Pb–17Li alloy at the velocities that have been studied), the corrosion mechanism can be divided into two steps:

(i) the dissolution reaction at the surface of the solid metal,

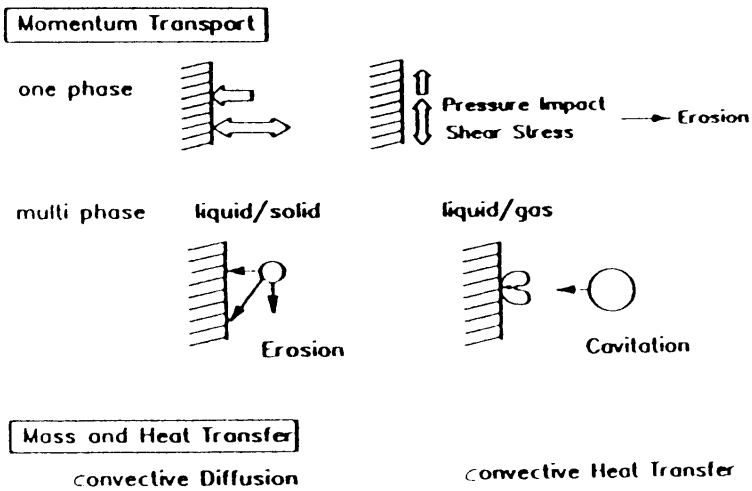

Fig. 2. Interactions of a flowing liquid with a solid boundary [17].

(ii) the transport by convective diffusion of the dissolved metal from the solid–liquid interface to the bulk:mass transfer.

At low velocities, the corrosion rate is completely or partially mass transfer controlled. In such a case, the global dissolution at the solid–liquid interface is at the equilibrium and the corrosion process is thus limited by the diffusion of the dissolved species in the laminar sublayer from the solid–liquid interface to the bulk (the corrosion rate corresponds to the mass transfer rate or diffusion flux). The thickness of the laminar sublayer depends on the hydrodynamic regime (geometry, fluid velocity, fluid physicochemical properties...). Therefore, when the corrosion process is mass transfer controlled, the corrosion rate increases with increasing velocity (phase B: 'mass transfer controlled' – Fig. 3). At high velocities, the dissolution reaction at the solid–liquid interface becomes the limiting step. In this region, the corrosion rate is independent of the fluid velocity and, in principle, also of the geometry (phase B: 'activation controlled' – Fig. 3). At much higher velocities, erosion–corrosion may occur if the surface shear stress is high enough to strip a protective film from the surface (phase C – Fig. 3) [5]. For heavy liquid metals, cavitation–corrosion is also likely to occur at high velocities due to their high density.

Most of the studies performed in liquid metals have shown a corrosion process controlled by mass transfer. However, the studied velocity range was quite narrow. For example, in the case of Pb–17Li, the maximum velocity of the alloy was 0.3 m s^{-1}. As said previously, it could reach 3 m s^{-1} in the spallation target, therefore the limiting step of the corrosion process could change for high velocities.

To study flow-induced corrosion, different experimental techniques are available

– the pipe flow tests,
– the rotating specimens (disc, cylinder,...),
– the jet impingement tests.

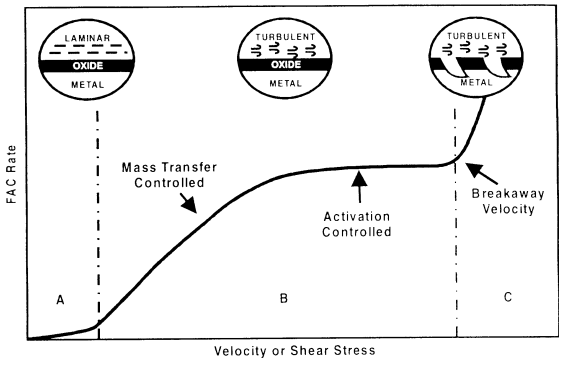

Fig. 3. Variation of the mechanism of flow accelerated corrosion (FAC) as a function of the fluid velocity [5].

Among these geometries, the rotating cylinder was selected for its specific characteristics:

– it generates turbulent convection for $Re > 100$, providing simulation conditions of this type of convection at relatively low rotation rates,
– the mass transfer equations are well-established,
– it allows quite small installations easy to handle,
– the corrosion results obtained on the rotating cylinder can be used to predict the behavior in other geometries.

The rotating cylinder also allows to determine the nature of the corrosion process. Depending on the law of the weight loss variation with the rotating rate, it is possible to establish if the corrosion process is limited by diffusion (the diffusion coefficient can be calculated) or by the dissolution step (the dissolution constant can be evaluated).

2.5. The rotating cylinder geometry: determination of the mass transfer coefficient

A recent review of the different equations that allow the estimation of the rotating cylinder velocities to simulate flow conditions in other geometries has been reported by Silverman [19]. The objective of this study was to determine which of the equations proposed in the literature might be the most appropriate. These models apply essentially in the case of mass transfer controlled corrosion.

For the rotating cylinder, the equation derived from the study of Eisenberg on the mass transfer of cylindrical nickel specimens in alkaline aqueous solutions tends to be used in most of the developments [20,21]. The mass transfer coefficient has been determined for turbulent flow and the expression is valid for Reynolds numbers between 10^3 and 10^5:

$$K_{\text{Eisenberg}} = 0.0487\omega^{0.70} d_{\text{cylinder}}^{0.4} v^{-0.344} D^{0.644},$$

where $K_{\text{Eisenberg}}$ is the mass transfer coefficient (m s^{-1}); ω is the rotation rate (rad s^{-1}); d_{cylinder} is the diameter of cylinder (m); v is the kinematic viscosity (m^2 s^{-1}); and D is the diffusion coefficient (m^2 s^{-1}).

Recently, a modification of this equation has been proposed by Maciel and Agostinho [22].

The authors performed corrosion tests with a 90 Cu–10 Ni alloy rotating cylinder immersed in HCl/Fe^{3+} medium. They minimized the end effects by installing inert ends. They obtained the following empirical law to express the mass transfer coefficient:

$$K_{\text{M-A}} = 0.0494\omega^{0.732} d_{\text{cylinder}}^{0.432} v^{-0.344} D^{0.644}.$$

This equation is close to the Eisenberg equation and does not imply important changes in the value of the mass transfer coefficient. Therefore, only the Eisenberg equation will be considered in our study.

Finally, the mass transfer rate expresses itself as

$$J = K(c - c_0)$$

with c as the wall concentration (g m^{-3}), the interface reaction is assumed to be rapid, therefore c is considered equal to the saturation concentration, $c \approx c_s$.

c_0 is the bulk concentration (g m^{-3}), in all cases, the fluid is assumed to be sufficiently renewed, therefore $c_0 \approx 0$.

Then, if we consider the Eisenberg mass transfer coefficient

$$J = K_{\text{Eisenberg}} c_s,$$

$$J = 0.0487\omega^{0.70} d_{\text{cylinder}}^{0.4} v^{-0.344} D^{0.644} c_s.$$

Assuming a mass transfer controlled corrosion process, the variation of the weight loss of the rotating cylinder is thus linear with $\omega^{0.70}$.

2.6. The pipe flow: determination of the mass transfer coefficient

It is assumed that the corrosion process is mass transfer controlled.

By equalizing the mass transfer coefficients established for a pipe flow geometry and for a rotating cylinder, a relationship is obtained which links the fluid velocity in the pipe to the cylinder rotation rate in order to attain equivalent mass transfer and corrosion rate in both geometries. Therefore, it is possible to predict the corrosion in a pipe from the results obtained on a rotating cylinder.

Several equations (all empirical) have been proposed to calculate the mass transfer coefficient in a pipe geometry. Silverman [19] reviewed the different equations and selected two of them (for smooth pipes) that, according to him, were established with the most reliable and representative results.

The first equation was developed by Berger and Hau using the mass transfer controlled ferricyanide/ferrocyanide reaction on pieces of nickel tube with a polished inner surface ensuring a roughness of about 1 μm [23]. The mass transfer coefficients were measured in fully developed flow for $8 \times 10^3 < Re < 2 \times 10^5$ at Schmidt numbers varying between 1000 and 6000:

$$K_{\text{B–H}} = 0.0165 v^{0.86} d_{\text{pipe}}^{-0.14} \nu^{-0.530} D^{0.670},$$

where v is the flow velocity (m s^{-1}); d_{pipe} is the inside diameter of specimen; ν is the kinematic viscosity (m^2 s^{-1}); and D is the diffusion coefficient (m^2 s^{-1}).

This equation was used by Nesic who examined corrosion of low carbon steel in CO_2 environments [12]. Comparison of the two different flow geometries, rotating cylinder and pipe flow, was carried out in terms of the hydrodynamics, mass transfer rates and corrosion mechanisms. The measured mass transfer rates were found to agree well with previous correlations obtained for the rotating cylinder and straight pipe flow. It was also possible to achieve good agreement between corrosion rates in the two flow geometries by ensuring the same mass transfer conditions.

The second equation, developed by Silverman, relies on the determination of the wall shear stress and friction velocity for high Sc, and Re up to $\sim 10^5$ [8,9]. He considered the friction velocity ($v^* = \sqrt{f/2}v$) as scaling velocity instead of the bulk velocity because, for high Schmidt number systems, the mass transfer boundary layer lies well within the hydrodynamic boundary layer. Using measurements made with the ferricyanide/ferrocyanide reaction under fully developed turbulent flow on a pipe wall that was polished smooth and coated with platinum, Silverman obtained the mass transfer coefficient:

$$K_{\text{Silverman}} = 0.0177 v^{0.875} d_{\text{pipe}}^{-0.125} \nu^{-0.579} D^{0.704}.$$

The Silverman and the Berger and Hau equations lead to very similar results. According to Silverman, they are based on the most representative and reliable results [19].

Although not selected by Silverman, another equation established by Harriott and Hamilton was considered in our study which, in some cases, represents efficiently the mass transfer in a pipe flow geometry [24]. The mass transfer coefficient is

$$K_{\text{H–H}} = 0.0096 v^{0.913} d_{\text{pipe}}^{-0.087} \nu^{-0.567} D^{0.654}.$$

Again, assuming the corrosion process is mass transfer controlled, the corrosion rate is expressed by the mass transfer rate:

$$J = K(c - c_0),$$

where c is the wall concentration (g m^{-3}), equal to the saturation concentration $c \approx c_s$; and c_0 is the bulk concentration (g m^{-3}), $c_0 \approx 0$.

With the expression of the mass transfer coefficient, it is possible to relate the weight loss to the velocity of the fluid.

The different expressions of the mass transfer coefficient for the pipe flow geometry and the rotating cylinder geometry are summarized in Table 2. It is important to note that, in all cases, the knowledge of the diffusion coefficient of the relevant species is essential to determine the relation between the different flow geometries.

The validity of these different equations is analyzed hereafter in the case of liquid metals and, more precisely, with the lead–lithium alloy for which experimental results are available for both the pipe and rotating cylinder geometries.

Table 2
Selected equations to determine the mass transfer coefficient K in (m s^{-1}) for a rotating cylinder and a pipe geometry

Rotating cylinder	Pipe
$K_{Eisenberg} = 0.0487\omega^{0.70} d_{cylinder}^{0.4} v^{-0.344} D^{0.644}$ [20,21]	$K_{B-H} = 0.0165 v^{0.86} d_{pipe}^{-0.14} v^{-0.530} D^{0.670}$ [23]
	$K_{Silverman} = 0.0177 v^{0.875} d_{pipe}^{-0.125} v^{-0.579} D^{0.704}$ [8,9]
	$K_{H-H} = 0.0096 v^{0.913} d_{pipe}^{-0.087} v^{-0.567} D^{0.654}$ [24]

3. Corrosion of steels in flowing liquid lead–lithium

3.1. Experimental corrosion data in Pb–17Li

3.1.1. Loop measurements

The composition of the materials tested in the different experiments is given in Table 3.

Among the numerous corrosion tests performed in pipe loops in the presence of flowing Pb–17Li, a part was selected for the validation of the model in order to have homogeneous results with a sufficient number of points (Table 4). The corrosion tests in loops were performed on cylindrical samples placed in pipes: the flow is not a simple pipe flow but an annular flow. The expressions of the mass transfer coefficient in an annular flow can be considered as similar to those determined for a pipe flow but the specific length becomes the hydraulic diameter instead of the inner pipe diameter [9]. The definition of the hydraulic diameter is: $d_h = d_2 - d_1$ where d_2 is the inner diameter of the pipe and d_1 is the external diameter of the cylindrical sample.

The following criteria are selected:

– Material: 1.4914 martensitic steel (Table 3).

– Temperature range: $T = 475$–500°C. In this range, the variation of parameters such as diffusion coefficient, solubility or kinematic viscosity is considered as negligible. For all the calculations of this study, the values of these parameters will be taken at 500°C.

The data used in the calculations are the following:

– temperature: $T = 500$°C,

– kinematic viscosity of Pb–17Li at 500°C: $v = 1.25 \times 10^{-7}$ m^2 s^{-1} [25],

– solubility of iron in Pb–17Li at 500°C: $c_s =$ 47 ppm = 439.45 g m^{-3} [26],

– in all cases c_0 is assumed to be negligible, $c_0 = 0$.

Concerning the value of the Fe solubility in Pb–17Li, discrepancies exist in the literature and two very different values are reported. A value was proposed by Borgstedt, close to the solubility of iron in pure lead [27,28]. The determination of this data was performed using corrosion tests results which revealed a dissolution mechanism of iron and chromium at constant rates. The corrosion rate was expressed according to

$$\dot{r} = K(c_s - c_0),$$

where $\dot{r}$ is the corrosion rate (μm h^{-1}), K is the mass transfer coefficient (m s^{-1}), c_s and c_0 are the atomic fractions, respectively, of the saturation concentration of

Table 3
Composition of the steels tested in the different experiments (wt%) [1,41]

Steel	C	Mn	Si	Cr	Mo	Ni	V	Nb
1.4914	0.13	0.82	0.37	10.6	0.77	0.87	0.22	0.16
Z 10 CD Nb V 92	0.105	1.03	0.37	9.65	2.04	–	0.32	0.46
10 CD 9–10	0.085	0.5	0.3	2.09	1.09	–	–	–

Table 4
Selected literature data on the corrosion rate of 1.4914 martensitic steel in a pipe loop geometry for different Pb–17Li velocities

Temperature T (°C)	Pb–Li velocity v_{pipe} (m s^{-1})	Hydraulic diameter d_h (m)	Corrosion rate (μg m^{-2} s^{-1})	Reference
475	0.019	0.022	4.9	[1]
475	0.08	0.0167	10.1	[45]
475	0.18	0.022	24.0	[1]
500	0.3	0.007	31.8	[27]

the dissolving metal in the liquid metal and the bulk concentration ($c_0 \approx 0$). The mass transfer coefficient is determined from an expression of the Sherwood number for a turbulent flow through a straight pipe [27]:

$$K = 0.037 v^{0.75} d^{-0.25} \nu^{-0.33} D^{-0.58}.$$

In this expression, the value of the diffusion coefficient is unknown for iron in lead–lithium, therefore Borgstedt assumed it to be equal to the diffusion coefficient of iron in pure lead. Knowing $\dot{r}$ and K, it is possible to determine c_s. A tentative equation restricted to the temperature range 450–600°C was established for Fe:

$$\log_{10} c_s[\text{mol\%}] = 7.236 - 9345 T^{-1}[\text{K}^{-1}].$$

At 500°C, $c_s = 1.40 \times 10^{-5}$ mol%. Therefore, the saturation concentration of Fe in Pb–17Li is $c_s = 0.044$ wppm (in pure lead, at 500°C, $c_s = 0.11$–3 wppm depending on the literature data).

The value of the solubility of iron in Pb–17Li proposed by Sample, Barker and Coen was very different [26,29]. They performed immersion tests of pure metals in Pb–17Li to determine the concentration of the dissolved metal in the liquid alloy using atomic absorption spectroscopy. These experiments were carried out at different temperatures and an expression of the variation of the Fe solubility with temperature was established:

$$\log_{10} c_s[\text{wppm}] = 2.524 - 655.0 T^{-1}[\text{K}^{-1}].$$

At 500°C, the value of the solubility of iron in Pb–17Li is about 47 wppm (1000 times higher than the $c_s = 0.044$ wppm value proposed by Borgstedt).

In our work, the value determined by Sample, Barker and Coen was selected. Borgstedt used corrosion tests results to determine solubility data. It is not a direct measurement of the saturation concentration and it is necessary to use a hydrodynamic model to determine the mass transfer coefficient in the expression of the corrosion rate. Moreover, this model requires the knowledge of the diffusion coefficient of iron in Pb–17Li. This data being undetermined, Borgstedt had to derive it from the value of the iron diffusion coefficient in pure lead corrected with a viscosity factor. All these assumptions increase the uncertainty on the determination of the solubility data. Sample et al. performed direct measurements of the dissolved metal concentration in Pb–17Li, the only uncertainty being the detection limits of the spectrometer used for the analysis. Therefore, their value was preferred for the calculations of the present study.

3.1.2. Rotating cylinder measurements

Among the corrosion tests performed in Pb–17Li with a rotating cylinder, two series performed at 500°C on 1.4914 martensitic steel are selected [30,31].

The first series was performed by Simon [30]. During the experiments, difficulties were observed: large areas of the steel were not wetted with Pb–17Li, giving an imperfect contact with the liquid alloy. The initial weight loss calculated on the total metallic surface was thus corrected and calculated with respect to the wetted surface.

To avoid these wetting problems, other tests were performed including a pre-wetting step of the samples at 550°C [31]. After these tests, an improvement of the wetting was noticed and large non-wetted areas were no longer observed. However, a correction of the weight loss had to be performed to take into account the dissolution undergone by the samples after the pre-wetting stage (maximum dissolution = 0.5 mg). The results obtained on the rotating cylinder are gathered in Table 5.

3.2. Experimental determination of the diffusion coefficient of iron in Pb–17Li

3.2.1. Loop measurements

The corrosion mechanism of 1.4914 martensitic steel in flowing liquid Pb–17Li is assumed to be a dissolution mechanism limited by the diffusion of iron in the laminar sublayer [1].

Table 5
Selected literature data on the corrosion rate of 1.4914 martensitic stainless steel in Pb–17Li at 500°C in a rotating cylinder geometry for different rotation rates

ω (rpm)	Measured corrosion rate ($\mu g\ m^{-2}\ s^{-1}$)	Corrected corrosion rate ($\mu g\ m^{-2}\ s^{-1}$): correction on the wetted surface
Series 1 [30]		
200	7.6	23.3
1000	29.7	55.8
ω (rpm)	Measured corrosion rate ($\mu g\ m^{-2}\ s^{-1}$)	Corrected corrosion rate ($\mu g\ m^{-2}\ s^{-1}$): correction on the weight loss after the pre-wetting step
Series 2 [31]		
200	6.5	5.2
500	13.5	12.5
1000	20.8	19.8

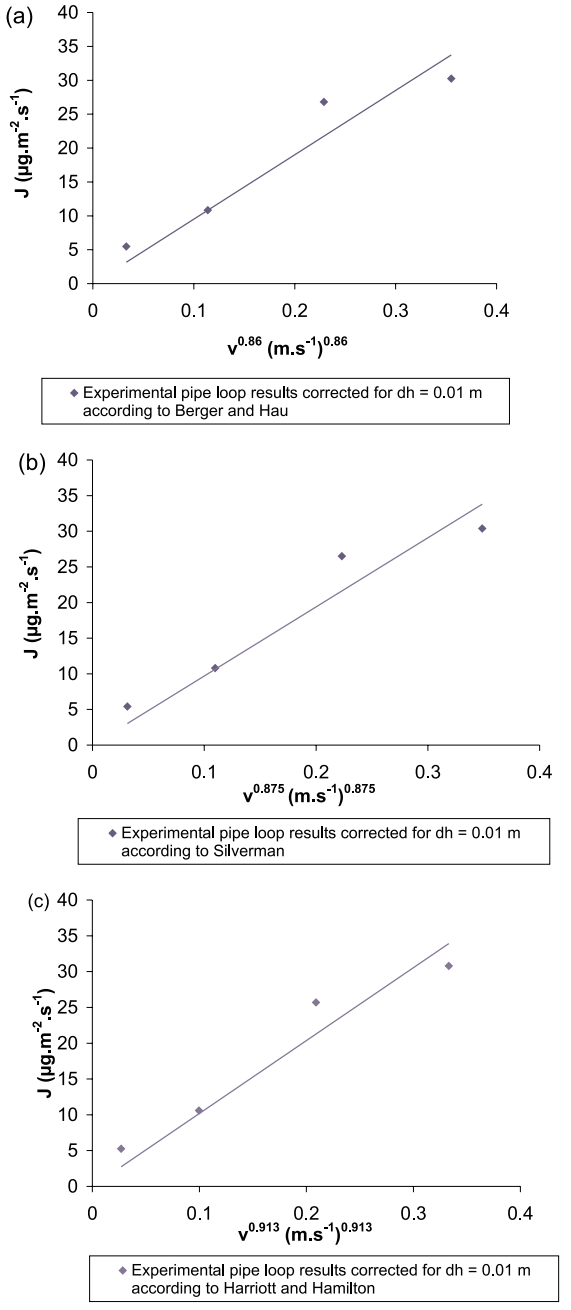

Fig. 4. Variation of the corrosion rate in pipe loops as a function of the Pb–17Li velocity corrected for $d_h = 0.01$ m according to the Berger and Hau equation (a), the Silverman equation (b), and the Harriott and Hamilton equation (c) – $T = 500$°C.

In all the equations presented to calculate the mass transfer coefficient (Table 2), the diffusion coefficient of the dissolved species is needed. Using the data of Table 4, it is possible to calculate the diffusion coefficient of Fe in Pb–17Li from the three different equations expressing the mass transfer coefficient.

To establish a graphic representation of the variation of the corrosion rate with the fluid velocity, it is necessary to make a correction on the hydraulic diameter in order to have all the corrosion rates determined for the same hydraulic conditions. Therefore, for each equation of the mass transfer coefficient, the corrosion rate is calculated for a hydraulic diameter equal to: $d_h = 0.01$ m (Table 6). Fig. 4 represents the results obtained. In all cases, the variation of the corrosion rate is linear with the fluid velocity which confirms the mass transfer control of the corrosion process.

The diffusion coefficients deduced from the slopes of the three curves are presented in Table 6.

3.2.2. Rotating cylinder measurements

Fig. 5 represents the variation of the corrosion rate (diffusion flux) with the rotation rate at the power 0.7 (corresponding to the Eisenberg equation) using the results of Table 5. If the corrosion process is mass transfer controlled, the diffusion flux must vary linearly with $\omega^{0.7}$. Although the experimental points are not numerous, the curves plotted agree with the mass transfer control of the corrosion process of the martensitic steel in Pb–17Li. The different values of the diffusion coefficients obtained from these curves are presented in Table 7.

3.2.3. Discussion on the diffusion coefficient of Fe in Pb–17Li

The different coefficients obtained via corrosion experiments by using the equations for both the pipe geometry and the rotating cylinder geometry have all the

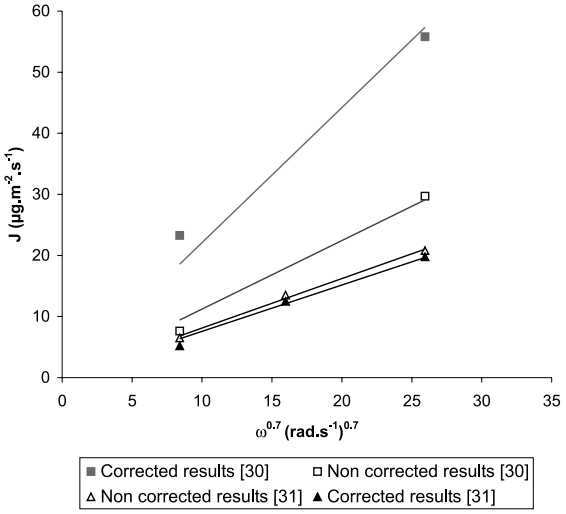

Fig. 5. Variation of the corrosion rate of a rotating cylinder immersed in Pb–17Li as a function of the rotating speed – $T = 500$°C.

Table 6
Determination of the diffusion coefficients of Fe in Pb–17Li at 500°C from the experimental pipe loop results, corrected for a hydraulic diameter equal to $d_h = 0.01$ m, and the three equations of the mass transfer coefficient

v (m s^{-1})	$J_{\text{corrected for B–H}}$ (μg m^{-2} s^{-1})	$D_{\text{B–H}}$ (m^2 s^{-1})	$J_{\text{corrected for Silverman}}$ (μg m^{-2} s^{-1})	$D_{\text{Silverman}}$ (m^2 s^{-1})	$J_{\text{corrected for H–H}}$ (μg m^{-2} s^{-1})	$D_{\text{H–H}}$ (m^2 s^{-1})
0.019	5.47	6.82×10^{-14}	5.41	1.00×10^{-13}	5.25	4.89×10^{-14}
0.08	10.85		10.8		10.6	
0.18	26.8		26.5		25.7	
0.3	30.25		30.4		30.8	

Table 7
Diffusion coefficients of iron in Pb–17Li at 500°C calculated from the rotating cylinder experiments using the Eisenberg equation

	$D_{\text{Eisenberg}}$ (m^2 s^{-1})
Corrected results [30] correction on the wetted surface	5.09×10^{-14}
Non-corrected results [30]	1.78×10^{-14}
Non-corrected results [31]	1.07×10^{-14}
Corrected results [31] correction on the weight loss after the pre-wetting step	9.67×10^{-15}

same order of magnitude, about 10^{-14} m^2 s^{-1}. However, this value is much smaller than the diffusion coefficient of iron in pure lead at 500°C: $D = 5.26 \times 10^{-10}$ m^2 s^{-1} [32] and also much smaller than usual diffusion coefficients reported in liquid metals (about 10^{-10}–10^{-9} m^2 s^{-1} [33]).

If the Sutherland–Einstein equation is used to determine a theoretical diffusion coefficient of iron in Pb–17Li, the following expression is obtained [34]:

$$D_{\text{Fe}\rightarrow\text{Pb–17Li}} = \frac{kT}{4\mu_{\text{Pb–17Li}} r_{\text{Fe}} \pi},$$

where D is the diffusion coefficient (m^2 s^{-1}), k is the Boltzmann constant (J K^{-1}), T is the temperature (K), μ is the viscosity of the medium (Pa s) and r (m) is the radius of the diffusing particle.

r_{Fe} can be calculated with the formula:

$$r_{\text{Fe}} = \frac{1}{2}\left[\frac{3V_{\text{Fe}}}{\pi N}\right]^{\frac{1}{3}},$$

where V_{Fe} is the molecular volume of iron at the temperature T and N is the Avogadro number [34]. At 500°C, $\mu_{\text{Pb–17Li}} = 1.18 \times 10^{-3}$ Pa s and $V_{\text{Fe}} = 7.24 \times 10^{-6}$ m^3 mol^{-1} [35] then $r_{\text{Fe}} = 1.13 \times 10^{-10}$ m.

Therefore, the diffusion coefficient of iron in Pb–17Li at 500°C deduced from the Sutherland–Einstein equation is: $D_{\text{Fe}\rightarrow\text{Pb–17Li}} = 6.4 \times 10^{-9}$ m^2 s^{-1}, which is much higher than the experimentally measured diffusion coefficient.

Several interpretations can be given to explain this difference

– The value of the iron solubility in Pb–17Li remains uncertain. Assuming a lower value in the diffusion flux expression, as the one proposed by Borgstedt [27,28], the diffusion coefficient would have been much higher. At 500°C, $D_{\text{Fe}\rightarrow\text{Pb–17Li}} = 2.57 \times 10^{-9}$ m^2 s^{-1} for $c_s = 0.044$ wppm $= 0.411$ g m^{-3}. This value is very close to the expected one. However, the solubilities determined by Borgstedt and recently reported by Feuerstein et al. [36] seem very low if we refer to studies carried out in our laboratory where analyses of Pb–17Li in loops operating between 250°C and 400°C indicated concentrations of iron close to 10 wppm. Such values are more in agreement with those reported in [26,29]. Other experiments would be necessary to confirm the solubility data.

– The experimental method may be not completely reliable: underestimations of the weight loss can be obtained with the rotating cylinder due to imperfect wetting or insufficient purification of the liquid alloy. For both geometries, convection movements may also interfere with the measurements. It is obvious that technical parameters have to be carefully designed to ensure relevant and reproducible experimental conditions. Such problems are not encountered in pipe loops where tests are much longer and purification systems are installed. Despite that, the diffusion coefficient values measured in pipe loops and with the rotating cylinder system are very close. Therefore, technical problems alone cannot explain such a difference between the measured diffusion coefficient and the one calculated with the Sutherland–Einstein equation.

– The corrosion process of the steel may not be controlled by mass transfer or only partially. However the variation of the corrosion rate agrees with a mass transfer controlled process: it is linear with the fluid velocity (Fig. 4) and with the rotation rate (Fig. 5) according to the equations proposed in Table 2. Moreover, the fact that the diffusion of iron is the limiting step has been confirmed by tests performed with pure iron: weight losses measured with pure iron are similar to those obtained with the martensitic steel.

– The models used to calculate the diffusion coefficient may not be representative of this specific medium. However, for very different couples (diffusing species/liquid metal) such as iron in liquid copper, calcium carbide in carbon-saturated iron melts, and also in different media like cryolitic melts, the use of the rotating cylinder led to satisfying results.
– The diffusing species may be much larger than an atom, leading to a higher radius: iron may not diffuse as a single atom but more obviously as a 'solvated' species with atoms of the solvent Pb–17Li.

Experimental measurements of the diffusion coefficient of iron in Pb–17Li have led to much smaller values than expected. Therefore, uncertainties remain concerning the determination of the diffusivity although the corrosion process of 1.4914 steel in Pb–17Li has been shown to be mass transfer controlled and it has been proven that the diffusion of iron is the controlling step. More experiments would be necessary to ensure the diffusion data. However, there is no question about the use of the mass transfer coefficient models in both geometries as they lead to the same results and represent the behavior of the steel in the liquid alloy in a reliable way.

Finally, one value of the diffusion coefficient of iron in liquid Pb–17Li at 500°C has to be selected for the calculations of the mass transfer coefficients. The experimental results obtained on the rotating cylinder and the Eisenberg equation will be preferentially used as in the case of the pipe flow, the most representative equation of the mass transfer coefficient in our experimental conditions has not yet been determined.

The experiments performed with the rotating cylinder led to various results depending on the experimental procedure. In the frame of this work, the value of the diffusion coefficient obtained by Simon with the corrected results [30] is chosen: $D = 5.09 \times 10^{-14}$ m^2 s^{-1} (Table 7). It is the highest value measured with the rotating cylinder experiments and, as the different uncertainties on the measurements tend to underestimate the diffusion coefficient, this datum was selected. Moreover, recent experiments performed on a 1.4914 martensitic steel rotating cylinder at 517°C led to a value of $D = 2$–6×10^{-14} m^2 s^{-1}, which is quite consistent with the selected value [37].

Table 8
Mass transfer coefficients calculated for the rotating cylinder geometry according to the Eisenberg equation in Pb–17Li at 500°C

ω (rad s^{-1})	$J_{exp.}$ (μg m^{-2} s^{-1})	$K_{Eisenberg}$ (m s^{-1})
20.94	23.3	4.18×10^{-8}
104.7	55.8	1.29×10^{-7}

3.3. Modeling analysis: determination of the best appropriate equation to calculate the mass transfer coefficient for a pipe flow

In this section, the experimental results considered for the rotating cylinder geometry are the corrected results of Simon [30] (corrected according to the wetted surface, Table 5). They are coherent with the selected value of the iron diffusion coefficient in Pb–17Li equal to 5.09×10^{-14} m^2 s^{-1} (Table 7).

From this diffusion coefficient, the mass transfer coefficient in a rotating cylinder geometry can be calculated (Table 8) for each rotation rate according to the Eisenberg equation:

$$K_{Eisenberg} = 0.0487\omega^{0.70} d_{cylinder}^{0.40} v^{-0.344} D^{0.644}.$$

For the pipe loop experiments, the mass transfer coefficients calculated from the three equations reported in Table 2 are presented in Table 9. To determine which equation of the mass transfer coefficient in pipe gives the best corrosion behavior of samples in contact with flowing Pb–17Li, the variation of the corrosion rate (measured in pipe loops and with the rotating cylinder) is plotted as a function of the mass transfer coefficient calculated with the different equations for the two flow geometries (Fig. 6).

The linearity between the corrosion rate and the mass transfer coefficient is observed. It confirms the mass transfer controlled corrosion process for both geometries (cf. Section 3.2.3).

It is shown that the corrosion rate measured in different Pb–17Li hydrodynamic configurations is independent of the geometry when plotted as a function of the mass transfer coefficient calculated from the Harriott–Hamilton equation (Fig. 6(c)): the same slope is obtained which corresponds to the solubility of iron in liquid Pb–17Li. The Berger and Hau equation (Fig. 6(a))

Table 9
Mass transfer coefficients calculated for the pipe flow geometry according to the Berger and Hau equation, the Silverman equation and the Harriott and Hamilton equation in Pb–17Li at 500°C

v (m s^{-1})	d_h (m)	$J_{exp.}$ (μg m^{-2} s^{-1})	K_{B-H} (m s^{-1})	$K_{Silverman}$ (m s^{-1})	K_{H-H} (m s^{-1})
0.019	0.022	4.9	5.27×10^{-9}	3.87×10^{-9}	5.97×10^{-9}
0.08	0.0167	10.1	1.89×10^{-8}	1.41×10^{-8}	2.27×10^{-8}
0.18	0.022	24.0	3.65×10^{-8}	2.77×10^{-8}	4.65×10^{-8}
0.3	0.007	31.8	6.64×10^{-8}	5.00×10^{-8}	8.19×10^{-8}

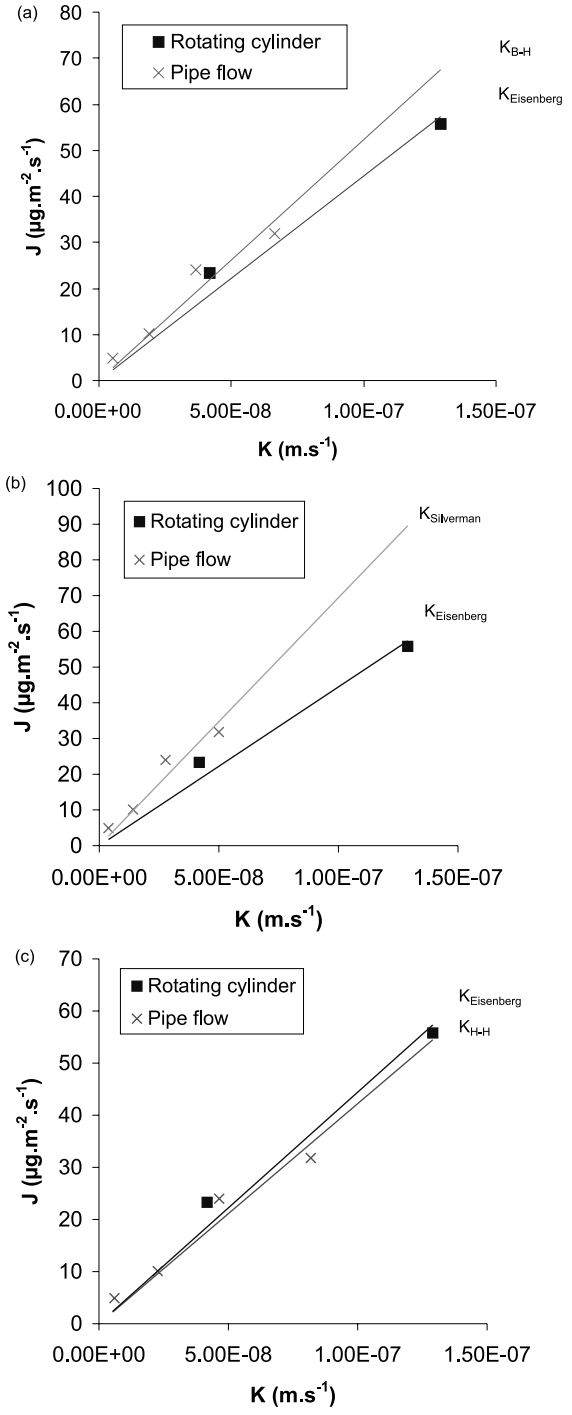

Fig. 6. Variation of the corrosion rate with the mass transfer coefficient calculated in Pb–17Li for the rotating cylinder according to the Eisenberg equation and for the pipe flow according to the Berger and Hau equation (a), the Silverman equation (b), and the Harriott and Hamilton equation (c) – $T = 500$°C.

also leads to a rather good agreement with the rotating cylinder experiments. This implies that corrosion data can be transferred from one geometry to another via mass transfer coefficients.

This analysis shows that the empirical equations of the mass transfer coefficients established in aqueous medium can effectively be used in liquid metal environments and more precisely with the liquid eutectic Pb–17Li. Concerning this specific medium, an uncertainty remains on the value of the diffusion coefficient of iron and other experimental techniques should be used to verify this result.

4. Corrosion of steels in flowing liquid lead

Experimental results of corrosion tests performed in pipe loops are available in pure liquid lead. No tests have been carried out with a rotating cylinder, however the three equations proposed to calculate the mass transfer coefficient in a pipe flow geometry (Table 2) can be used: (i) to determine if the results obtained by calculations agree with those of the experiments, (ii) to determine which equation is the best to represent the corrosion behavior in flowing liquid lead.

Tests were performed in oxygen-free lead so that dissolution of the steel occurs in the liquid metal.

A first test performed with iron samples in a forced convection loop led to a corrosion rate equivalent to 2600 µm yr^{-1} [38]. The pure lead circulated at 0.42 m s^{-1} and the temperature in the hot leg was 600°C. The corrosion process is assumed to be mass transfer controlled.

The following parameters are considered:

– temperature: $T = 600$°C,
– fluid velocity: $v = 0.42$ m s^{-1},
– inside diameter of the pipe: $d_{\text{pipe}} = 0.01$ m (estimated value),
– kinematic viscosity of Pb at 600°C: $v = 1.545 \times 10^{-7}$ m^2 s^{-1} [39],
– diffusion coefficient of iron in pure liquid lead at 600°C: $D = 1.15 \times 10^{-9}$ m^2 s^{-1} [32],
– solubility of iron in Pb at 600°C: $c_s = 2.44$ ppm $= 25.1$ g m^{-3} [40].

According to the three equations (Table 2), the values of the mass transfer coefficient are

$K_{\text{B–H}} = 6.22 \times 10^{-5}$ m s^{-1},
$K_{\text{Silverman}} = 6.59 \times 10^{-5}$ m s^{-1},
$K_{\text{H–H}} = 6.73 \times 10^{-5}$ m s^{-1}.

Then, the corrosion rate, $J = Kc_s$, is equal to

$J_{\text{B–H}} = 1.56 \times 10^{-3}$ g m^{-2} s^{-1} $= 6255$ µm yr^{-1},
$J_{\text{Silverman}} = 1.65 \times 10^{-3}$ g m^{-2} s^{-1} $= 6627$ µm yr^{-1},
$J_{\text{H–H}} = 1.69 \times 10^{-3}$ g m^{-2} s^{-1} $= 6768$ µm yr^{-1}.

The three equations give similar values, the closest to the experimental value being obtained with the Berger and Hau equation. The calculated corrosion rate is

approximately 2.4 times higher than the measured value. It has to be noted that this type of modeling leads to an overestimation of the corrosion rate as it will be discussed in Section 5. Despite this deviation, experimental and calculated results remain reasonably close.

Another series of tests was performed in pure lead on two steels (10 CD 9-10 and Z 10 CD Nb V 92, Table 3) in a thermal convection loop at a temperature of 550°C. The lead velocity was about 0.1 m s^{-1}. The corrosion rate was in the range 70–120 μm yr^{-1} for Z 10 CD Nb V 92 and 220–320 μm yr^{-1} for 10 CD 9–10 [41].

The following parameters are considered:

– temperature: $T = 550$°C,
– fluid velocity: $v = 0.10$ m s^{-1},
– inside diameter of the pipe: $d_{pipe} = 2.47 \times 10^{-2}$ m,
– kinematic viscosity of Pb at 550°C: $v = 1.65 \times 10^{-7}$ m^2 s^{-1} [42],
– diffusion coefficient of iron in liquid lead at 550°C: $D = 7.97 \times 10^{-10}$ m^2 s^{-1} [32],
– solubility of iron in Pb at 550°C: $c_s = 1.41$ ppm = 14.5 g m^{-3} [40].

The mass transfer coefficient calculated from the three equations are

$K_{B-H} = 1.21 \times 10^{-5}$ m s^{-1},
$K_{Silverman} = 1.25 \times 10^{-5}$ m s^{-1},
$K_{H-H} = 1.27 \times 10^{-5}$ m s^{-1}.

It can be deduced that the corrosion rate, $J = Kc_s$, is

$J_{B-H} = 1.75 \times 10^{-4}$ g m^{-2} s^{-1} = 691 μm yr^{-1}
$J_{Silverman} = 1.81 \times 10^{-4}$ g m^{-2} s^{-1} = 714 μm yr^{-1}
$J_{H-H} = 1.84 \times 10^{-4}$ g m^{-2} s^{-1} = 726 μm yr^{-1}.

The maximum experimental corrosion rate was 320 μm yr^{-1} and the calculations give a value around 700 μm yr^{-1}. Again, the calculated values are overestimated (about two times higher than the measurements) but this deviation remains reasonable.

Although the three expressions of the mass transfer coefficient lead to very close results, the best corresponding equation seems to be the Berger and Hau equation. In the following, this equation will preferentially be used for the calculations but the approach is exactly the same for the other equations.

As with the Pb–17Li alloy, the results obtained by using the mass transfer coefficients in pure liquid lead for the pipe flow geometry are quite satisfying even if the predicted corrosion rates remain higher than the experimental values. It can be concluded that this method for predicting the corrosion rates is applicable for liquid lead alloys when the corrosion process is mass transfer controlled.

5. Estimation of the corrosion of steels in flowing liquid lead–bismuth

The corrosion process in liquid Pb–Bi can proceed according to two mechanisms depending on the oxygen concentration [15]:

– If the oxygen content is lower than a critical minimum value (≈ 10^{-8} wt% at 500°C), the corrosion process is similar to the one occurring in Pb–17Li: the steel dissolves in the liquid alloy and a mass transfer control process can be assumed at least for moderate velocities. In that case, the same equations as those presented above can be applied.
– If the oxygen content is higher than 10^{-8} wt%, a protective oxide layer forms at the interface between the steel and the liquid alloy. In that case, the effect of the flow velocity on the behavior of the oxide layer has to be studied.

If the steel is exposed to Pb–Bi with a low oxygen content, the corrosion proceeds by dissolution and a mass transfer control can be assumed. The diffusion of iron is supposed to be the controlling step as for Pb–17Li. Therefore, the expressions of the mass transfer coefficient can be used to predict the corrosion rate for a rotating cylinder and for a pipe loop geometry. For the rotating cylinder, the Eisenberg equation is used whereas for the pipe geometry, the Berger and Hau equation is used.

The liquid metal velocities to be simulated vary from 0 to 5 m s^{-1} for a pipe diameter (hydraulic diameter) of 10 cm. In a first step, it is possible to determine the rotation rates of a cylinder (for a given geometry) to reproduce the same corrosion conditions as for the pipe geometry. As said previously, the diffusion coefficient is needed to calculate the mass transfer coefficient. Concerning the diffusion coefficient of iron in liquid Pb–Bi, a single value has been found in the literature: $D_{(Fe \to Pb-Bi)}$ at 750°C = $2.27 \pm 0.11 \times 10^{-9}$ m^2 s^{-1} [38]. The value of the diffusion coefficient of iron in lead at 750°C is estimated to: $D_{(Fe \to Pb)} = 2.80 \times 10^{-9}$ m^2 s^{-1} [32]. For a given temperature, the values of the diffusion coefficient of iron in Pb or Pb–Bi are quite close. Therefore, the diffusion coefficient of iron in Pb–Bi at 500°C is assumed to be equal to the one measured in lead: $D_{(Fe \to Pb)} = 5.26 \times 10^{-10}$ m^2 s^{-1} = $D_{(Fe \to Pb-Bi)}$.

For the calculations, different rotating cylinder diameters are considered. The experimental parameters are:

– temperature: $T = 500$°C,
– internal diameter of the pipe: $d_{pipe} = 0.1$ m,
– external diameter of the cylinder: $d_{cylinder} = [0.5\text{-}1\text{-}2\text{-}3\text{-}4\text{-}5] \times 10^{-2}$ m,
– kinematic viscosity of Pb–Bi at 500°C: $v = 1.284 \times 10^{-7}$ m^2 s^{-1} [42],
– diffusion coefficient of iron in Pb–Bi at 500°C: $D_{(Fe \to Pb-Bi)} = 5.26 \times 10^{-10}$ m^2 s^{-1},
– solubility of iron in Pb–Bi at 500°C: $c_s = 22.21$ g m^{-3} [43].

If the mass transfer coefficients expressed for both geometries ($K_{Eisenberg} = 0.0487\omega^{0.70}d_{cylinder}^{0.40}v^{-0.344}D^{0.644}$ and $K_{B-H} = 0.0165v^{0.86}d_{pipe}^{-0.14}v^{-0.530}D^{0.670}$) are equalized, it is possible to determine the corresponding rotation rate

Table 10
Values of the cylinder rotation rate to obtain similar mass transfer coefficients in a pipe geometry as a function of the pipe velocity and cylinder diameter in liquid Pb–Bi at 500°C

v (m s^{-1})	$d_{cylinder}$ (m)					
	0.005	0.01	0.02	0.03	0.04	0.05
0.5	873	588	396	314	266	235
1	2047	1378	928	736	624	550
2	4798	3230	2174	1725	1464	1288
3	7898	5318	3579	2839	2409	2121
4	11 247	7571	5096	4043	3431	3020
5	14 796	9960	6705	5319	4513	3973

and linear velocity to obtain the same diffusion flux (corrosion rate) in both geometries.

The rotation rate ω can be expressed as

$$\omega = 0.213 v^{1.229} d_{pipe}^{-0.2} d_{cylinder}^{-0.571} v^{-0.266} D^{0.0371}.$$

Table 10 gives the values of the cylinder rotation rate (in rpm) as a function of the pipe velocities and cylinder diameters.

Due to technological problems, rotating over 8000 rpm is complex. Therefore, diameters between 0.005 and 0.01 m cannot be used to simulate velocities up to 5 m s^{-1} as they imply a rotation rate higher than 8000 rpm. Furthermore, in each tests two cylinders are fixed at the stirring system. If the samples are too heavy, perturbations can occur and destabilize the stirring shaft. Thus, diameters of 0.04 and 0.05 m are eliminated. Finally, a cylinder diameter of 0.03 m appears satisfying to carry out experiments in representative and safe conditions.

The cylinder diameter being selected, corrosion rates can be evaluated with the expressions of the mass transfer coefficients in a pipe geometry or a rotating cylinder for equivalent rotation speeds and pipe flow velocities.

According to the Eisenberg equation:

$$J = K_{Eisenberg} c_s = 0.0487 \omega^{0.70} d_{cylinder}^{0.40} v^{-0.344} D^{0.644} c_s.$$

The mass transfer coefficient and the corrosion rate can be calculated as a function of the angular velocity and linear velocity (Table 11). The estimated corrosion rate may be overestimated as the value of the diffusion coefficient of iron in liquid Pb–Bi at 500°C is not precisely known. Moreover, some assumptions made in the modeling can lead to an overestimation of the corrosion rate [44]:

– The assumption that the liquid metal is saturated at the interface ($c = c_s$) leads in all cases to an overestimation of the corrosion rate.

– The bulk concentration is assumed equal to zero ($c_0 = 0$) but in real cases the concentration can increase with time and may even tend to the saturation concentration.

Fig. 7 compares the variation of the diffusion flux with the mass transfer coefficient (calculated with the Berger and Hau equation for the pipe flow and with the Eisenberg equation for the rotating cylinder) in Pb–17Li and in Pb–Bi. For a same mass transfer coefficient, the corrosion rate measured in Pb–17Li is higher than the corrosion rate predicted in Pb–Bi: this is due to the solubility of iron which is higher in Pb–17Li than in Pb–Bi. For a same liquid metal velocity, the mass transfer coefficients calculated in Pb–17Li are much lower than those calculated in Pb–Bi, which is explained by the extremely low value of the diffusion coefficient of iron in Pb–17Li compared to the one reported in Pb–Bi. Therefore, it is necessary to be very careful when using the mass transfer coefficient to compare the corrosion behavior in different media as it takes into account physico-chemical properties of the medium, geometric properties of the installation and also diffusion properties of the dissolved metal.

Table 11
Mass transfer coefficients and corrosion rates calculated with the Berger and Hau equation and the Eisenberg equation as a function of the rotation rate and of the corresponding pipe velocity in Pb–Bi at 500°C for $d_{pipe} = 0.1$ m and $d_{cylinder} = 0.03$ m

v_{pipe} (m s^{-1})	ω (rpm)	K (m s^{-1})	J (μg m^{-2}s^{-1}) – J (μm yr^{-1})
0.5	314	3.43×10^{-5}	761.5–3002
1	736	6.22×10^{-5}	1383–5452
2	1725	1.13×10^{-4}	2510–9894
3	2839	1.60×10^{-4}	3557–14,022
4	4043	2.05×10^{-4}	4556–17,960
5	5319	2.49×10^{-4}	5521–21,764

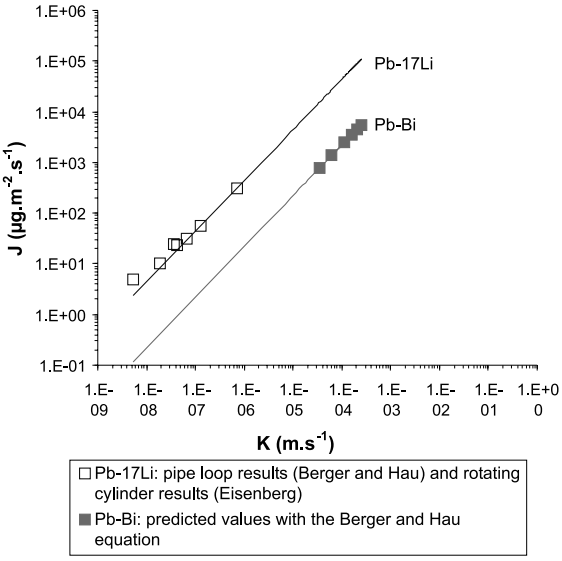

Fig. 7. Comparison of the corrosion rate versus the mass transfer coefficient (calculated with the Berger and Hau equation for the pipe loop geometry and the Eisenberg equation for the rotating cylinder) in Pb–17Li and in Pb–Bi – $T = 500$°C. (logarithmic scale).

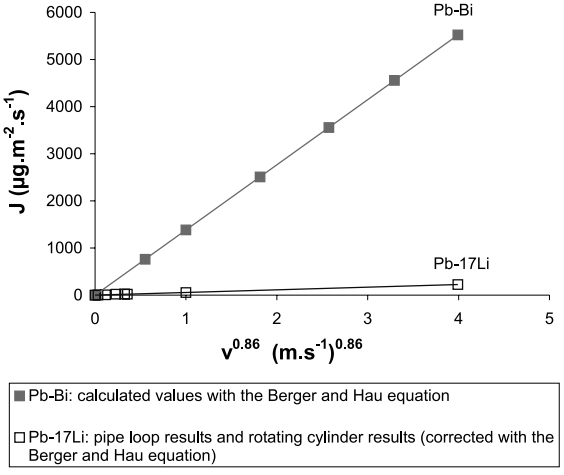

Fig. 8. Comparison of the corrosion rate versus the liquid metal velocity in Pb–17Li and in Pb–Bi (for Pb–17Li, the experimental results are corrected with the Berger and Hau equation to obtain the same hydraulic diameter: $d_h = 0.1$ m) – $T = 500$°C.

If the corrosion rate is directly represented as a function of the liquid metal velocity (Fig. 8), we observe that the corrosion rate is much higher in Pb–Bi than in Pb–17Li: even if iron is very soluble in Pb–17Li, it diffuses very slowly therefore the corrosion rate is globally lower than in Pb–Bi for a same liquid metal velocity.

These calculations give a very preliminary evaluation of the Pb–Bi velocity effect on the dissolution of steels. Up to now, information is lacking about the corrosion rate of steels in Pb–Bi and experiments are necessary to validate the first prediction and to determine the controlling step of the corrosion process. In this work, calculations have been performed assuming a mass transfer controlled corrosion process but at high velocities the controlling step could be the surface reaction. Other mechanisms such as erosion–corrosion or cavitation–corrosion could also be considered.

6. Conclusion

For practical evaluation of the effect of fluid velocity on corrosion of steels in the Pb–Bi spallation target, the use of a rotating cylinder operating under controlled hydrodynamics is of interest. It is shown that the models developed in aqueous medium to simulate the hydrodynamic conditions in a pipe flow geometry from a rotating cylinder geometry can effectively be used in the case of liquid metals such as Pb–17Li and Pb provided that the corrosion proceeds by dissolution and is mass transfer controlled.

The corrosion rate measured in the two different hydrodynamic systems (pipe flow and rotating cylinder) is independent of the geometry when plotted as a function of the mass transfer coefficient. Therefore, results generated with a rotating cylinder can be used to make predictions about corrosion in a real liquid metal flow. All that is needed are the appropriate equations giving the mass transfer coefficient. It has to be noted that the knowledge of the diffusion coefficient as well as the solubility of the dissolved species in the liquid is essential to transfer the corrosion data from one geometry to another.

In the Pb–Bi alloy with a low oxygen content (corrosion proceeds by dissolution), the Berger and Hau equation and the Harriott and Hamilton equation are considered for the pipe flow geometry whereas the Eisenberg equation is selected for the rotating cylinder geometry. Nevertheless, experimental measurements of corrosion rates on a rotating cylinder and on samples in pipe flow are needed to validate these equations and ultimately to use them for predicting the corrosion behavior of steels in the spallation module.

Finally, a complete study of the Pb–Bi system would necessitate to examine the case when corrosion of steel proceeds by oxidation (high oxygen content in Pb–Bi). In such conditions, the oxide formed on the surface can protect the steel against dissolution. This point was not investigated in the present paper but experiments and models for determining the behavior of the oxide layer under various hydrodynamic conditions should also be

considered to prevent degradation phenomena of the protective layer.

References

[1] J. Sannier, T. Flament, A. Terlain, Fus. Technol. (1990) 901.
[2] Y. Poitevin, J. Bergeron, J.P. Deffain, R. Enderle, R. Lenain, J. Raballand, Design and limitations of the spallation module for an hybrid system dedicated to waste incineration, 3rd AccApp, Long Beach, California, USA, 14–18 November 1999.
[3] F. Balbaud, F. Barbier, in: J. Könys (Ed.), Minutes of the Workshop on Heavy Liquid Metal Technology, Karlsruhe, Germany, 16–17 September 1999, Forschungszentrum Karlsruhe, Germany, FZKA 6389, 1999.
[4] D.R. Gabe, G.D. Wilcox, J. Gonzalez-Garcia, F.C. Walsh, J. Appl. Electrochem. 28 (1998) 759.
[5] T.Y. Chen, A.A. Moccari, D.D. Macdonald, Corrosion 48 (1992) 239.
[6] B. Poulson, Corros. Sci. 23 (1983) 391.
[7] E. Heitz, G. Kreysa, C. Loss, J. Appl. Electrochem. 9 (1979) 243.
[8] D.C. Silverman, Corrosion 40 (1984) 220.
[9] D.C. Silverman, Corrosion 44 (1988) 42.
[10] R.A. Holser, G. Prentice, R.B. Pond Jr., R. Guanti, Corrosion 46 (1990) 764.
[11] K. Denpo, H. Ogawa, Corrosion 49 (1993) 442.
[12] S. Nesic, G.T. Solvi, J. Enerhaug, Corrosion 51 (1995) 773.
[13] B.T. Ellison, W.R. Schmeal, J. Electrochem. Soc. 125 (1978) 524.
[14] K.D. Efird, E.J. Wright, J.A. Boros, T.G. Hailey, Corrosion 49 (1993) 992.
[15] V. Markov, Seminar on the concept of lead-cooled fast reactors, Cadarache 22–23 September 1997, private communication.
[16] B. Chexal, J. Horowitz, Flow-accelerated corrosion in power plants, TR 106611, EDF-EPRI, Pleasant Hill, CA, 1996.
[17] E. Heitz, Corrosion 47 (1991) 135.
[18] J. Weber, Brit. Corros. J. 27 (1992) 193.
[19] D.C. Silverman, Corrosion 55 (1999) 1115.
[20] M. Eisenberg, C.W. Tobias, C.R. Wilke, J. Electrochem. Soc. 101 (1954) 306.
[21] M. Eisenberg, C.W. Tobias, C.R. Wilke, Chem. Eng. Prog. Symp. Ser. 51 (1954) 1.
[22] J.M. Maciel, S.M.L. Agostinho, J. Appl. Electrochem. 29 (1999) 741.
[23] F.P. Berger, K.-F.F.-L. Hau, Int. J. Heat Mass Transfer 20 (1977) 1185.
[24] P. Harriott, R.M. Hamilton, Chem. Eng. Sci. 20 (1965) 1073.
[25] U. Jauch, G. Haase, B. Schulz, Thermophysical properties in the system Li–Pb, Part II: Thermophysical properties of Li(17)Pb(83) eutectic alloy, Kernforschungszentrum Karlsruhe, Report KFK 4144, 1986.
[26] V. Coen, T. Sample, Fus. Technol. (1990) 248.
[27] H.U. Borgstedt, H.D. Röhrig, J. Nucl. Mater. 179–181 (1991) 596.
[28] H.U. Borgstedt, H. Feuerstein, J. Nucl. Mater. 191–194 (1992) 988.
[29] M.G. Barker, T. Sample, Fus. Eng. Des. 14 (1991) 219.
[30] N. Simon, PhD thesis, Paris VI University, 1992.
[31] T. Dufrenoy, private communication.
[32] W.M. Robertson, Trans. TMS-AIME 242 (1968) 2139.
[33] T. Iida, R.D.L. Guthrie, The Physical Properties of Liquid Metals, Clarendon, Oxford, 1988.
[34] C. Guminski, in: H.U. Borgstedt, G. Frees (Eds.), Liquid Metal Systems, Plenum, New York, 1995, p. 345.
[35] P. Pascal, New Treatise of Inorganic Chemistry, Masson, Paris, 1967.
[36] H. Feuerstein, H. Gräbner, J. Oschinski, J. Beyer, S. Horn, L. Hörner, K. Santo, Compatibility of 31 metals, alloys and coatings with static Pb–17Li eutectic mixture, Forschungszentrum Karlsruhe, FZKA 5596, 1995.
[37] T. Dufrenoy, private communication.
[38] S. Banerjee, in: Proceedings of the Fifth International Congress on Metallic Corrosion, Tokyo, Japan, May 21–27, NACE, Houston, Texas, 1974.
[39] G. Lemercier, private communication.
[40] J.R. Weeks, A.J. Romano, Corrosion 25 (1969) 131.
[41] J. Sannier, G. Santarini, J. Nucl. Mater. 107 (1982) 196.
[42] R.R. Miller in: R.N. Lyon (Ed.), Liquid Metals Handbook, US Government Printing Office, Washington, 1954, p. 38.
[43] P.N. Martynov, K.D. Ivanov, in: Nuclear heat applications: design aspects and operating experiences – Proceedings of four technical meetings held between December 1995 and April 1998, IAEA, Vienna, Austria, 1998, p. 177.
[44] S. Malang, D.L. Smith, Modeling of Liquid Metal Corrosion/Deposition in a Fusion Reactor Blanket, Argonne National Laboratory, Report ANL/FPP/TM-192, 1984.
[45] T. Flament, P. Fauvet, B. Hocde, J. Sannier, Fus. Technol. (1988) 1184.